How Much Physics is in a Current–Voltage Curve? Inferring Defect Properties From Photovoltaic Device Measurements

Rachel C. Kurchin, Jeremy R. Poindexter, Ville Vähänissi, Hele Savin, Carlos del Cañizo, and Tonio Buonassisi, *Member, IEEE*

***Abstract*—Defect-assisted recombination processes are critical to understand, as they frequently limit the photovoltaic (PV) device performance. However, the physical parameters governing these processes can be extremely challenging to measure, requiring specialized techniques and sample preparation. And yet the fact that they limit performance as measured by current–voltage (*JV*) characterization indicates that they must have some detectable signal in that measurement. In this work, we use numerical device models that explicitly account for these parameters alongside high-throughput *JV* measurements and Bayesian inference to construct probability distributions over recombination parameters, showing the ability to recover values consistent with previously reported literature measurements. The Bayesian approach enables easy incorporation of data and models from other sources; we demonstrate this with temperature dependence of carrier capture cross-sections. The ability to extract these fundamental physical parameters from standardized, automated measurements on completed devices is promising for both established industrial PV technologies and newer research-stage ones.**

***Index Terms*—Bayesian parameter estimation (BPE), crystalline silicon, high-performance computing (HPC), high-throughput experiment (HTE), iron contamination, Shockley–Read–Hall (SRH) recombination.**

Manuscript received December 18, 2019; revised February 21, 2020, April 8, 2020, May 29, 2020, and July 9, 2020; accepted July 13, 2020. The work of J. R. Poindexter was supported by the Switzer Environmental Fellowship. This work was supported by the Center for Next Generation Materials by Design (CNGMD), an Energy Frontier Research Center funded by the U.S. Department of Energy, Office of Science, Basic Energy Sciences, as well as the MIT-Spain—Universidad Politécnica de Madrid Seed Fund. *(Corresponding author: Rachel C. Kurchin.)*

Rachel C. Kurchin is with the Massachusetts Institute of Technology, Cambridge, MA 02139 USA, and also with the Carnegie Mellon University, Pittsburgh, PA 15213 USA (e-mail: rkurchin@alum.mit.edu).

Jeremy R. Poindexter is with the Massachusetts Institute of Technology, Cambridge, MA 02139 USA, and also with the Tesla Inc., Fremont, CA 94538 USA (e-mail: jpoindex@alum.mit.edu).

Ville Vähänissi and Hele Savin are with the Department of Electronics and Nanoengineering, Aalto University, 02150 Espoo, Finland (e-mail: ville.vahanissi@aalto.fi; hele.savin@aalto.fi).

Carlos del Cañizo is with the Instituto de Energía Solar, Universidad Politécnica de Madrid, 28040 Madrid, Spain (e-mail: Carlos.canizo@ies.upm.es).

Tonio Buonassisi is with the Massachusetts Institute of Technology, Cambridge, MA 02139 USA (e-mail: buonassisi@mit.edu).

Color versions of one or more of the figures in this article are available online at http://ieeexplore.ieee.org.

Digital Object Identifier 10.1109/JPHOTOV.2020.3010105

I. Introduction

RECOMBINATION mediated by point defects is a performance-limiting mechanism in many photovoltaic (PV) technologies [1]–[3]. Identifying and characterizing these defects are essential to mitigating their effects. Typically, defect characterization is performed on wafers or semifabricates using temperature- and/or injection-dependent lifetime spectroscopy (TIDLS) [4], [5], deep level transient spectroscopy (DLTS) [6]–[8], and related spectroscopy techniques. However, these techniques are time-consuming, and the deep expertise necessary to master them is rare. Measurements on semifabricates may not be representative of finished devices, as final processing can affect defect populations. With the maturation of data-science methods, we explore the possibility of extracting defect information directly from nondestructive electrical device measurements.

Any defects detrimental to the device performance should by definition have a signature in the device performance such as current–voltage (*JV*) measurements. However, such a signal is convoluted with those from so many other physical processes that it cannot be extracted or interpreted through a simple fitting approach, as the fit would be underconstrained. However, by combining current–voltage measurements at a range of temperatures and light intensities (*JVTi*) with physics-based device models [9]–[11] and Bayesian statistics, these signals can be disentangled, providing fits for many types of underlying parameters, often with greater precision than direct characterization allows.

We previously demonstrated this Bayesian parameter estimation (BPE) approach to measure materials properties such as minority carrier mobility and lifetime in a finished tin sulfide solar cell [12]. The Bayesian framework enables quantifying parameter-specific uncertainty as well as observing emergent relationships between parameters (such as mobility-lifetime product in [12]). In this work, we apply this approach to extract defect-assisted recombination parameters for interstitial iron in silicon, obtaining results consistent with reported literature values. Our results demonstrate a novel approach to extract defect properties from inexpensive measurements of completed devices, demonstrating promise for characterization of both established and novel PV technologies.

II. Methods

Please note that supplemental information for this article is available at the repository for the analysis code: https://github.com/PV-Lab/Fe_Si_Bayes_code/blob/master/final_SI.pdf. References to supplementary figures refer to this document.

A. Experimental Methods

For this study, silicon solar cells were obtained from the same set used in previous work where samples were intentionally contaminated with specific amounts of interstitial iron (Fe_i); see [13] ("60 A" samples) for details regarding sample fabrication and measurements of iron concentration. Two of these samples were further characterized in this work: one intentionally contaminated sample with a known Fe_i concentration of 2×10^{12} cm^{-3} (after gettering), and a control sample with no intentional contamination (with estimated $[Fe_i] \leq 10^{10}$ cm^{-3}, based on measurement detection limits). Measurements were first performed on a 1-Sun (AM1.5 G, 1000 W/m^2) solar simulator setup (Newport Oriel Sol3A, class AAA, 450 W Xe lamp, AM1.5 G filter, Keithley 2400) to verify open-circuit voltage degradation of less than 1.5% rel. since the samples were first fabricated. Samples were aperture during all *JV* and *JVTi* measurements to ensure accurate short-circuit current values would be obtained. Quantum efficiency (QE) (PV Measurements QEX7, 300–1100 nm, 75 W Xe lamp, spectral products CM110 monochromator) and reflectance data (Perkin–Elmer Lambda 950 UV-Vis spectrophotometer, 150 mm integrating sphere) were also obtained for the purposes of fitting to the PC1D model (see in the following).

JVTi measurements were performed under vacuum (approx. 10^{-3}–10^{-5} Torr) using a liquid helium cryostat (ARS DE-204SI) and compressor (ARS-4HW) to reach colder sample temperatures while avoiding the condensation of atmospheric species; measurements were taken from 300 to 175 K at increments of 25 K. Precise temperature control within ± 1 K was achieved by placing a thermocouple (Omega CY670) directly on the sample surface and using a polyimide resistive heater (Minco HAP6943) and PID temperature controller (Lakeshore 331) to control total heat flux to the sample. Sample illumination at four different intensities (1.01, 0.69, 0.31, and 0.09 Suns, measured with a silicon photodiode) was achieved using a Newport Oriel solar simulator (LCS-100, class ABB, $1.5'' \times 1.5''$ uniform output) along with an array of neutral-density filters placed within two filter wheels (Thorlabs FW102 C). *JV* sweeps were performed using a Keithley 2400 sourcemeter. To ensure all iron present was in the form of Fe_i (versus Fe–B pairs), samples were soaked for 15 min at 1 Sun and 300 K before measurements began, as suggested from calculations of temperature-dependent re-pairing rates based on [14] and [15]. *JV* data at 300 K and 1 Sun illumination are shown in Fig. 1. For more *JV* data and figures of merit (open-circuit voltage, short-circuit current, fill factor), see Figures S3 and S4. Diffusion length measurements on a reference wafer performed concurrently with the work in [13] of 140 and 55 μm before and after a light soak, respectively, further support the assertion that Fe_i is the limiting defect. Furthermore, QE measurements (see Figure S5) show little difference between samples in the low wavelengths, indicating negligible differences in junction quality.

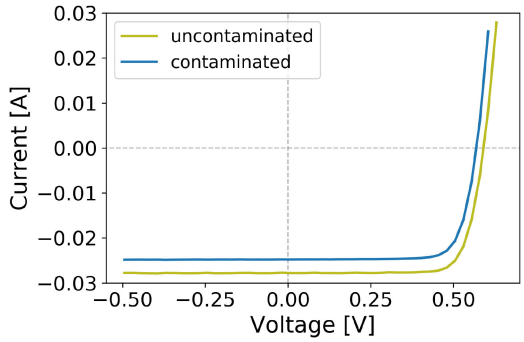

Fig. 1. Current versus voltage for uncontaminated and intentionally contaminated samples at 300 K and 1.01 Sun illumination.

B. Computational Methods

The 1-Sun *JV*, QE, and reflectance measurements were used to construct a numerical device model accessed by the Bayesian inference framework (see in the following). The use of a modified, command-line version of PC1D [9], [10] enabled scripted methods for modifying simulation parameters. Specific input parameters were obtained from previous measurements [13], estimated from literature values, or varied in the model to match the *JV*, QE, and reflectance data of the uncontaminated sample. A full list of device parameters is listed in the Supplementary Information (Tables S1-3).

For the three-parameter analyses at separate temperatures (shown in Fig. 2), BPE was performed on a (3D) grid of 36 logarithmically spaced points from 10^{-11} to 10^{-5} s in τ_n, 28 logarithmically spaced points from 10^{-5} to 10^{-1} s in τ_p, and 28 linearly spaced points spanning from the valence band maximum to the conduction band minimum (with energies referenced to the intrinsic Fermi level) in E_t. For the 5-parameter analysis, the grid consisted of 16 logarithmically spaced points from 10^{-19} to 10^{-15} cm^2 in σ_{n0}, 12 logarithmically spaced points from 10^{-16} to 10^{-13} cm^2 in σ_{p0}, 8 linearly spaced points from 0.15 to 0.23 eV in $E_{a,n}$, 9 linearly spaced points from -0.12 to -0.03 eV in $E_{a,p}$, and 16 linearly spaced points from the valence band maximum to 0.16 eV below the conduction band minimum in E_t.

Uniform priors (equal initial probability in every grid box) were used in each analysis; it is worth noting that with hundreds of experimental data points, the final outputs are not very sensitive to the choice of prior. Model uncertainty is estimated from numerical derivatives of model output along the parameter grid, and the standard deviation is taken as the maximum of the model uncertainty and the precharacterized experimental noise level. We used a modified Gaussian likelihood, wherein the argument was only ever evaluated as an integer number of standard deviations. This has the effect of spreading probability out along grid boxes and reducing incidence of artificially low probability densities arising from the maximally correct parameter space point lying near the edge of a box. This is especially important for the analysis undertaken here, where the output variable can vary extremely sensitively with the input parameters in certain regions of the parameter space.

These BPE calculations were performed using the Bayesim package, for more details see [16], the source code on

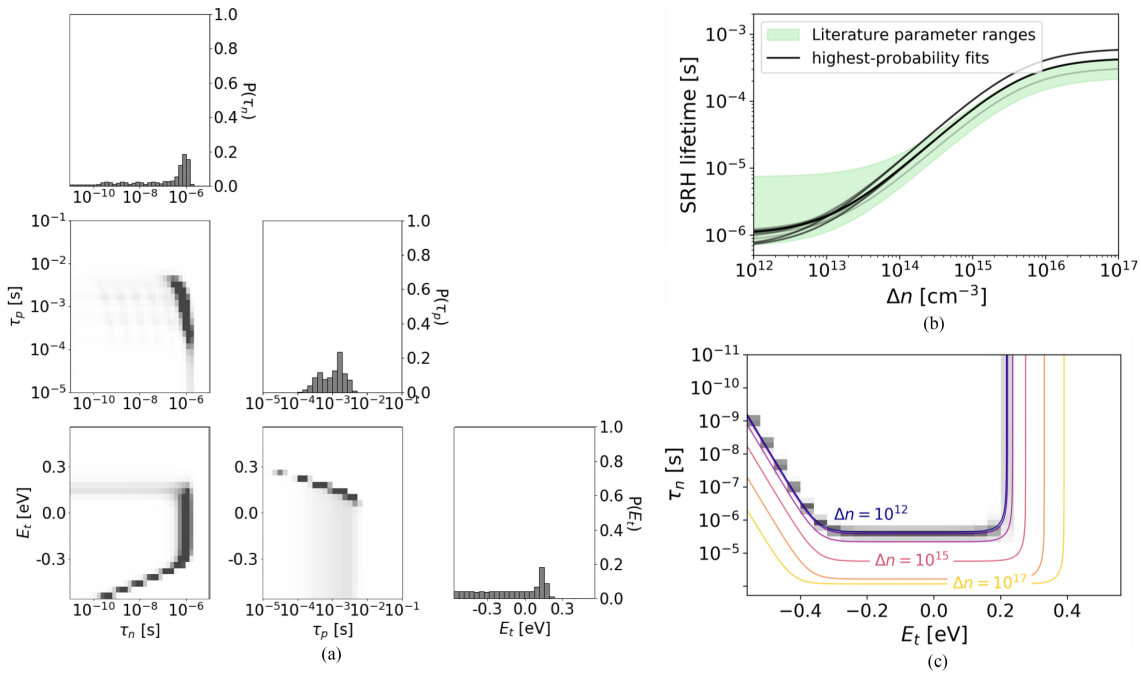

Fig. 2. Visualizations of results of three-parameter fit for contaminated sample at 300 K. (a) Probability distribution, with single-variable marginalizations along the diagonal and two-variable marginalizations off-diagonal. Two-variable marginalizations have increased contrast relative to defaults (with intensity of color proportional to square root of probability rather than its value) to better show shapes. (b) Simulated SRH lifetime versus injection for the highest probability sets of parameters. Intensity of lines proportional to probability, top 80 parameter sets (corresponding to 46% of total probability mass) shown. Green region shows simulated data based on ranges of parameters found in the literature. (c) Marginalization between E_t and τ_n from (a) (but with default visualization contrast) with calculated iso-injection curves overlaid. Each curve differs from the next by a factor of 10.

Github,[1] and/or the package documentation.[2] PC1D simulations were run on MIT Supercloud [17] using Wine [18] and the LLMapReduce [19] function. Code to reproduce figures plotted herein also is available.[3]

III. Three-Parameter Fits at Separate Temperatures

Defect-assisted recombination is described by the Shockley–Read–Hall (SRH) [20], [21] equation, where the SRH lifetime τ_{SRH} is given by

$$\tau_{\text{SRH}} = \frac{\tau_p \left(n + n_i \exp\left(\frac{E_t - E_i}{k_B T}\right)\right) + \tau_n \left(p + n_i \exp\left(\frac{E_i - E_t}{k_B T}\right)\right)}{np - n_i^2} \tag{1}$$

where n and p are the concentrations of electrons and holes, respectively, n_i is the intrinsic electron concentration, E_t is the energy level of the defect (trap), E_i is the intrinsic Fermi level, T is temperature, k_B is Boltzmann's constant, and the lifetime parameters τ_n and τ_p are given by

$$\tau_n = \frac{1}{N_t \sigma_n v_{\text{th},n}} \tag{2}$$

$$\tau_p = \frac{1}{N_t \sigma_p v_{\text{th},p}} \tag{3}$$

where N_t is the defect concentration, σ_n and σ_p are the defect capture cross sections for electrons and holes, respectively, and $v_{\text{th},n}$, $v_{\text{th},p}$ are the thermal velocities of electrons and holes, respectively.

Interstitial iron is one of the most detrimental (and hence, best characterized) point defects in silicon PV devices. In this work, we seek to characterize τ_n, τ_p, and E_t from *JVTi* measurements. Varying temperature and illumination intensity is critical to distinguish the influences of different defect parameters. These dependencies on experimental conditions are encoded in PC1D [9], [10], the device simulation software we chose for this study (For a visualization of the impact of various parameters, see Figure S1). In general, carrier concentrations depend linearly on light intensity. PC1D does not explicitly include temperature dependence of capture cross-sections; we account for this ourselves and the mathematical model is discussed as follows [see (4) and (5)].

Using *JV* measurements taken from 175–300 K and 0.09–1 Sun, we first construct posterior probability distributions (formally, because they are discrete, probability mass functions, or PMFs) over τ_n, τ_p, and E_t at each temperature separately. (See Methods section for discussion of special likelihood function to capture the correct iso-probability-density curve shapes.) An example (at 300 K) is plotted in Fig. 2(a) (See Figures S6 and S7 for what this plot would look like with data from only one voltage point and only one illumination level, respectively). Note that, as expected, this PMF does not show a unique high-probability point, as it has been well-established in the literature [4], [22] that without measurements at multiple temperatures and/or doping levels, the SRH equations do not have a unique solution. (We will incorporate data from multiple temperatures into a single fit in

[1]https://github.com/PV-Lab/bayesim
[2]https://pv-lab.github.io/bayesim/_build/html/index.html
[3]https://github.com/PV-Lab/Fe_Si_Bayes_code

the subsequent section, but this simpler analysis can nonetheless be illustrative.)

Next, we choose the highest-probability regions in this 3D parameter space and use them to construct simulated SRH lifetime curves as a function of carrier injection level, shown in Fig. 2(b). Also shown (in green) is the range corresponding to the ranges of parameters reported in the literature [4], [23] and constructed using tabulated values for thermal velocities in silicon [24] and previously characterized defect densities on this sample [13]. The simulated curves from this study are generally within the literature ranges (see discussion below regarding disagreement at high injection).

Fig. 2(c) shows the marginal distribution between τ_n and E_t from Fig. 2(a), with iso-injection curves overlaid. These were constructed using a fixed τ_p value for the purposes of visualization, chosen as roughly the center (i.e., logarithmic average) of the high-density region in Fig. 2(a). τ_{SRH} was fixed to the logarithmic average over the range computed from literature parameters in Fig. 2(b), and then (1) was inverted to give a relationship between τ_n and E_t. The results are consistent with the fact that these devices should be in low injection under the illumination levels used. (Interestingly, in Fig. 2(b), we also see a better agreement with the literature in low injection, emphasizing the importance of data spanning all relevant conditions to get the best fit.) This analysis again demonstrates that similar information to lifetime spectroscopy can be gleaned from our approach.

IV. Five-Parameter Fit Across All Temperatures

As alluded to above, because thermal velocities in silicon are tabulated and trap density in this sample has been characterized, we can directly correspond the time constants τ_n and τ_p to capture cross sections [see (2) and (3)]. A widely accepted model for carrier capture is as a thermally activated process [23], [25]. Implementing such a model allows an Arrhenius relation to be used for each capture cross-section, introducing two new parameters for each carrier: a prefactor σ_0 and an activation energy E_a:

$$\sigma_n = \sigma_{n0} e^{E_{a,n}/k_B T} \tag{4}$$

$$\sigma_p = \sigma_{p0} e^{E_{a,p}/k_B T}. \tag{5}$$

The parameter space is now 5D, but we can also constrain a single posterior distribution using all the data rather than needing separate fits at each temperature. The full probability distribution resulting from this analysis is shown in Fig. S2. Moving forward, we focus on σ_p in literature data comparisons, because significantly more data has been reported than for σ_n. Fig. 3(a) shows an excerpt from Fig. S2, namely, the marginalization between $E_{a,p}$ and σ_{p0}. The line of similar posterior probability seen in Fig. 3(a) (note that σ_{p0} is logarithmically spaced) represents the inherent tradeoff between prefactor and activation energy when fitting an exponential model like this over a finite temperature range. This tradeoff is clear from Fig. 3(b), which shows the literature-sourced σ_p values at discrete temperatures as well as the lines corresponding to the highest-probability Arrhenius parameter sets from this analysis. See Fig. S3 for comparisons between modeled and observed *JV* data at all sets of experimental conditons. Literature values are from [26]–[32] and were originally collated by [23]; acquisition methods include DLTS, thermally stimulated capacitance (a predecessor technique to DLTS), and Hall effect.

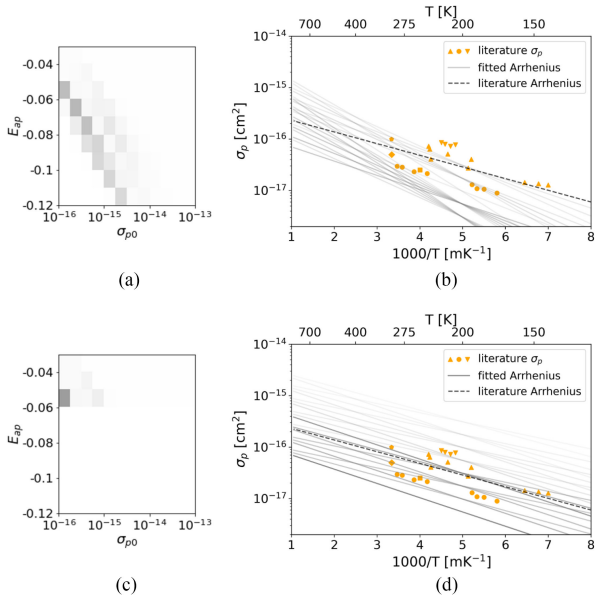

Fig. 3. (a) $E_{a,p}$–σ_{p0} marginalization from five-parameter Arrhenius fit. (b) σ_p data from literature ([23], [26]–[32]) with inferred Arrhenius fits, intensity of line proportional to probability of parameters, and Arrhenius fit from the literature [23]. (c) Marginalization from (a) conditioned on $E_{a,p}$ value being within. 01 eV of the literature value of -0.045 eV. (d) Same plot as (b) but for the marginalized PMF from (c). [top 20 Arrhenius fit parameter sets plotted in both (b) and (d)].

The dotted line in Fig. 3(b) represents the Arrhenius fit from [23]. However, that fit allowed only the prefactor to vary, fixing the activation energy according to the results of a separate measurement, while in our analysis we allowed the activation energy to be a fitting parameter. A strength of the Bayesian approach is that information from such a measurement can be explicitly incorporated via conditioning the posterior distribution further. To do this, we simply set the probability to zero in all grid boxes that do not have activation energies near this value (-0.045 eV), then renormalize the overall distribution. After this operation, Fig. 3(a) becomes (c), and (b) becomes (d), with the results agreeing even more closely with the literature fit.

V. Conclusion

In this work, we demonstrate the ability to extract SRH recombination parameters from device-level measurements (rather than characterization of semifabricates) and BPE utilizing a modified Gaussian likliehood that yields comparable results to TIDLS and DLTS. In particular, our results fall well within the range of values reported by different DLTS practitioners, and simulated IDLS data are also in agreement. However, our approach utilizes a much simpler and more widely applicable experimental setup—a temperature-controlled *JV* stage with a solar simulator and neutral-density filters, making defect characterization potentially accessible to a broader range of researchers, including those investigating earlier-stage materials. Furthermore, *JV* measurement is a standard industrial characterization technique, meaning this approach could be integrated into

manufacturing environments where samples from production lines could be tested using this technique to provide valuable feedback into impurities introduced during the manufacturing process, potentially utilizing sample heating rather than (or in addition to) cooling to remove the need for a cryostat. It also shifts a significant number of person-hours of effort to computational resources, which are becoming increasingly inexpensive, plentiful, and user-friendly. In addition, the Bayesian framework allows easy incorporation of any preexisting information from other sources, such as (in this work) parametrization of thermal velocity or prior characterization of trap density or capture barrier. We note that within the range of experimental conditions of our measurements (in particular, all measurements being in the low-injection regime), we were not able to significantly constrain the trap level. This would likely be resolved with a setup capable of concentrated measurements significantly above 1 Sun of illumination. Another interesting direction in this regard would be applying the BPE approach to Suns-V_{oc} measurements.

In this study, we investigated a system (interstitial iron in crystalline silicon) for which parameters have been extensively reported in the literature to allow for validation of results. We believe that this approach could be used for identification of unknown defects provided that there is reasonable confidence of one defect dominating the SRH signal (a frequent but not universal occurrence). However, if multiple defects were present, it is likely that some prior knowledge constraining their parameters relative to each other would be needed, as it has been shown that unambiguous identification of two defects is not feasible in all cases [33].

We emphasize that in any analysis of this kind, the quality of the results obtained is strictly bounded above by the applicability of the model whose parameters are being estimated. For example, if in reality the temperature dependence of capture cross sections deviates from a thermally activated model, the meaning of the associated parameters and their probability distributions could be called into doubt as well. (Some authors [34], [35] have also suggested a power law relationship between capture cross section and temperature.)

This work represents a simple, rapid [$\mathcal{O}$(1 day) each experiment time and simulation time on a sufficient high-performance computing (HPC) cluster] approach to access SRH parameters from finished devices, which promises to be useful both in screening of novel PV materials as well as characterizing better-known ones, as defect parameter data are generally very sparse in the literature due to the complexity of its collection.

Acknowledgment

The authors would like to thank the MIT SuperCloud and Lincoln Laboratory Supercomputing Center for providing HPC and consultation resources that have contributed to the research results reported within this article and would like to thank the provision of facilities and technical support by Aalto University at OtaNano—Micronova Nanofabrication Centre, and the Academy of Finland Flagship Programme, Photonics Research and Innovation (PREIN), and also would like to thank A. Istratov and Z. Liu for helpful discussions, H. Laine for assistance with sample procurement, and L. Milechin for assistance integrating Wine with LLMapReduce on the Supercloud system.

References

[1] M. Schubert *et al.*, "Iron related solar cell instability: Imaging analysis and impact on cell performance," *Sol. Energy Mater. Sol. Cells*, vol. 138, pp. 96–101, 2015. [Online]. Available: https://linkinghub.elsevier.com/retrieve/pii/S0927024815001026

[2] A. Collord, H. Xin, and H. W. Hillhouse, "Combinatorial exploration of the effects of intrinsic and extrinsic defects in $Cu_2ZnSn(S,Se)_4$," *IEEE Trans. Electron Devices*, vol. 5, no. 1, pp. 288–298, Jan. 2015.

[3] K. Durose, "High efficiency for As-doped cells," *Nature Energy*, vol. 4, no. 10, pp. 825–826, 2019. [Online]. Available: http://www.nature.com/articles/s41560-019-0475-2

[4] S. Rein, T. Rehrl, W. Warta, and S. W. Glunz, "Lifetime spectroscopy for defect characterization: Systematic analysis of the possibilities and restrictions," *J. Appl. Phys.*, vol. 91, no. 3, pp. 2059–2070, 2002.

[5] A. E. Morishige *et al.*, "Lifetime spectroscopy investigation of light-induced degradation in p-type multicrystalline silicon PERC," in *Proc. IEEE 44th Photovolt. Specialist Conf.*, 2017, vol. 6, no. 6, pp. 1–7.

[6] D. V. Lang, "Deep-level transient spectroscopy: A new method to characterize traps in semiconductors," *J. Appl. Phys.*, vol. 45, no. 7, 1974, Art. no. 3023. [Online]. Available: http://scitation.aip.org/content/aip/journal/jap/45/7/10.1063/1.1663719

[7] N. M. Johnson, "Deep level transient spectroscopy: Defect characterization in semiconductor devices," *MRS Proc.*, vol. 69, pp. 75–94, 1986.

[8] D. Wickramaratne *et al.*, "Defect identification based on first-principles calculations for deep level transient spectroscopy," *Appl. Phys. Lett.*, vol. 113, no. 19, 2018, Art. no. 192106.

[9] H. Haug, J. Greulich, A. Kimmerle, and E. S. Marstein, "PC1Dmod 6.1—State-of-the-art models in a well-known interface for improved simulation of Si solar cells," *Sol. Energy Mater. Sol. Cells*, vol. 142, pp. 47–53, 2015. [Online]. Available: https://linkinghub.elsevier.com/retrieve/pii/S0927024815002640

[10] H. Haug and J. Greulich, "PC1Dmod 6.2—Improved simulation of c-Si devices with updates on device physics and user interface," *Energy Procedia*, vol. 92, no. 1876, pp. 60–68, 2016. [Online]. Available: http://dx.doi.org/10.1016/j.egypro.2016.07.010

[11] M. Burgelman, P. Nollet, and S. Degrave, "Modelling polycrystalline semiconductor solar cells," *Thin Solid Films*, vol. 361–362, pp. 527–532, 2000. [Online]. Available: http://www.sciencedirect.com/science/article/pii/S0040609099008251

[12] R. E. Brandt *et al.*, "Rapid semiconductor device characterization through Bayesian parameter estimation," *Joule*, vol. 1, no. 4, pp. 843–856, 2017. [Online]. Available: https://doi.org/10.1016/j.joule.2017.10.001

[13] V. Vähänissi, A. Haarahiltunen, H. Talvitie, M. Yli-koski, and H. Savin, "Impact of phosphorus gettering parameters and initial iron level on silicon solar cell properties," *Prog. Photovolt.: Res. Appl.*, vol. 21, no. 5, pp. 1127–1135, 2013.

[14] D. Macdonald, T. Roth, P. N. K. Deenapanray, T. Trupke, and R. A. Bardos, "Doping dependence of the carrier lifetime crossover point upon dissociation of iron-boron pairs in crystalline silicon," *Appl. Phys. Lett.*, vol. 89, no. 14, 2006, Art. no. 142107. [Online]. Available: http://aip.scitation.org/doi/10.1063/1.2358126

[15] G. Zoth and W. Bergholz, "A fast, preparation–free method to detect iron in silicon," *J. Appl. Phys.*, vol. 67, no. 11, pp. 6764–6771, 1990. [Online]. Available: http://aip.scitation.org/doi/10.1063/1.345063

[16] R. Kurchin, G. Romano, and T. Buonassisi, "Bayesim: A tool for adaptive grid model fitting with Bayesian inference," *Comput. Phys. Commun.*, vol. 239, pp. 161–165, 2019. [Online]. Available: https://doi.org/10.1016/j.cpc.2019.01.022

[17] A. Reuther *et al.*, "Interactive supercomputing on 40,000 cores for machine learning and data analysis," in *Proc. IEEE High Perform. Extreme Comput. Conf.*, 2018, pp. 1–6. [Online]. Available: https://ieeexplore.ieee.org/document/8547629/

[18] "Wine." [Online]. Available: https://www.winehq.org, Accessed on: Jul. 28, 2020.

[19] C. Byun *et al.*, "LLMapReduce: Multi-level map-reduce for high performance data analysis," in *Proc. IEEE High Perform. Extreme Comput. Conf.*, 2016, pp. 1–8. [Online]. Available: http://ieeexplore.ieee.org/document/7761618/

[20] W. Shockley and W. T. Read, "Statistics of the recombination of holes and electrons," *Phys. Rev.*, vol. 87, no. 46, pp. 835–842, 1952.

[21] R. N. Hall, "Electron-hole recombination in germanium," *Phys. Rev.*, vol. 87, no. 2, 1952, Art. no. 387.

[22] J. D. Murphy, K. Bothe, R. Krain, V. Voronkov, and R. Falster, "Parameterisation of injection-dependent lifetime measurements in semiconductors in terms of Shockley-Read-Hall statistics: An application to oxide precipitates in silicon," *J. Appl. Phys.*, vol. 111, no. 11, 2012, Art. no. 113709.
[23] A. A. Istratov, H. Hieslmair, and E. R. Weber, "Iron and its complexes in silicon," *Appl. Phys. A*, vol. 44, pp. 13–44, 1999. [Online]. Available: https://doi.org/10.1007/s003390050968
[24] M. A. Green, "Intrinsic concentration, effective densities of states, and effective mass in silicon," *J. Appl. Phys.*, vol. 67, no. 6, pp. 2944–2954, 1990.
[25] R. Pässler, "Temperature dependences of the nonradiative multiphonon carrier capture and ejection properties of deep traps in semiconductors. I. Theoretical results," *Physica Status Solidi (b)*, vol. 85, no. 1, pp. 203–215, 1978. [Online]. Available: http://doi.wiley.com/10.1002/pssb.2220850122
[26] H. Lemke, "Doping properties of iron in silicon," *Physica Status Solidi (a)*, vol. 64, no. 1, pp. 215–224, 1981. [Online]. Available: http://doi.wiley.com/10.1002/pssa.2210640123
[27] H. Lemke, "For the detection of recombination centers in the bases of Si rectifiers," *Physica Status Solidi (a)*, vol. 63, no. 1, pp. 127–136, 1981. [Online]. Available: http://doi.wiley.com/10.1002/pssa.2210630117
[28] K. Wünstel and P. Wagner, "Interstitial iron and iron-acceptor pairs in silicon," *Appl. Phys. A Solids Surfaces*, vol. 27, no. 4, pp. 207–212, 1982. [Online]. Available: http://link.springer.com/10.1007/BF00619081
[29] S. D. Brotherton, P. Bradley, and A. Gill, "Iron and the iron–boron complex in silicon," *J. Appl. Phys.*, vol. 57, no. 6, pp. 1941–1943, 1985. [Online]. Available: http://aip.scitation.org/doi/10.1063/1.335468
[30] H. Indusekhar and V. Kumar, "Properties of iron related quenched-in levels in p-silicon," *Physica Status Solidi (a)*, vol. 95, no. 1, pp. 269–278, 1986. [Online]. Available: http://doi.wiley.com/10.1002/pssa.2210950134
[31] X. Gao, H. Mollenkopf, and S. Yee, "Annealing and profile of interstitial iron in boron–doped silicon," *Appl. Phys. Lett.*, vol. 59, no. 17, pp. 2133–2135, 1991. [Online]. Available: http://aip.scitation.org/doi/10.1063/1.106103
[32] S. Rein and S. W. Glunz, "Electronic properties of interstitial iron and iron-boron pairs determined by means of advanced lifetime spectroscopy," *J. Appl. Phys.*, vol. 98, no. 11, 2005, Art. no. 113711.
[33] T. U. Narland, S. Bernardini, M. S. Wiig, and M. I. Bertoni, "Is it possible to unambiguously assess the presence of two defects by temperature- and injection-dependent lifetime spectroscopy?" *IEEE J. Photovolt.*, vol. 8, no. 2, pp. 465–472, Mar. 2018.
[34] B. B. Paudyal, K. R. McIntosh, and D. H. Macdonald, "Temperature dependent electron and hole capture cross sections of iron-contaminated boron-doped silicon," in *Proc. 34th IEEE Photovolt. Specialists Conf.*, Jun. 2009, pp. 001588–001593.
[35] K. Graff, *Metal Impurities in Silicon-Device Fabrication* (Springer Series in Materials Science). Berlin, Germany: Springer-Verlag, 1995, no. 24.

Rachel C. Kurchin received the B.S. degree in physics (intensive) from Yale University, New Haven, CT, USA, in 2013, the M.Phil. degree inmaterials science and metallurgy from the University of Cambridge, Cambridge, U.K., in 2014, and the Ph.D. degree in materials science and engineering from the Massachusetts Institute of Technology, Cambridge, MA, USA, in 2019.

She is currently a Postdoctoral Fellow with Carnegie Mellon University, Pittsburgh, PA, USA, working on data science and machine learning for the optimization of fuel cells and next-generation lithium-ion batteries.

Jeremy R. Poindexter received the B.S. degree in mechanical engineering from Yale University, New Haven, CT USA, in 2011 and the Ph.D. degree in materials science and engineering from the Massachusetts Institute of Technology, Cambridge, MA, USA, in 2018.

His research has focused on performance-limiting mechanisms due to point defects in early-stage photovoltaic materials, as well as various optoelectronic characterization techniques such as time-resolved photoluminescence and quantum efficiency. He currently works as a Senior Process Development Engineer for Tesla.

Ville Vähänissi received the D.Sc. (Tech.) degree in semiconductor technology from Aalto University, Helsinki, Finland, in 2016.

He is currently working as a Staff Scientist with the Department of Electronics and Nanoengineering, Aalto University School of Electrical Engineering. His research interests include defect engineering in silicon, especially photovoltaics, as well as atomic layer deposition and its various applications in semiconductor devices.

Hele Savin received the D.Sc. (Tech.) degree in semiconductor technology from Aalto University, Finland, in 2005.

She is currently an Associate Professor with the Department of Electronics and Nanoengineering, Aalto University. Her research interests focus on material research in semiconductors, more specifically defect engineering in silicon, nanostructured silicon, light-induced degradation, and silicon photodetectors.

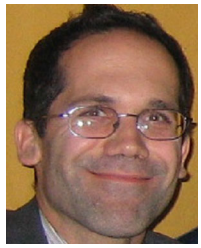

Carlos del Cañizo received a Ph.D. degree in telecommunication engineering at Universidad Politécnica de Madrid, in 2000. He is currently a Full Professor with the Universidad Politécnica de Madrid, Madrid, Spain, and the Director of its Solar Energy Institute. He has been involved in Photovoltaic research for more than 25 years, working on the manufacturing and characterisation of solar cells, on defect engineering techniques in silicon, and also in the field of silicon refinement.

Tonio Buonassisi (Member, IEEE) received the Ph.D. degree in applied science and technology from the University of California at Berkeley, Berkeley, CA, USA, in 2006.

He conducted the research with the Fraunhofer Institute for Solar Energy Systems, Freiburg, Germany, and the Max-Planck-Institute for Microstructure Physics, Halle, Germany. He is currently the Head of the Photovoltaic Research Laboratory, Massachusetts Institute of Technology, Cambridge, MA, USA, which combines machine learning, high-throughput experiments, and high-performance computing to accelerate the development of energy-relevant materials and systems. Thematic areas include processing, characterization, defects, and cost-performance modeling to engineer naturally abundant and manufacturable materials into cost-effective high-performance devices.

Supplementary Information for "How much physics is in a current-voltage curve? Inferring defect properties from photovoltaic device measurements"

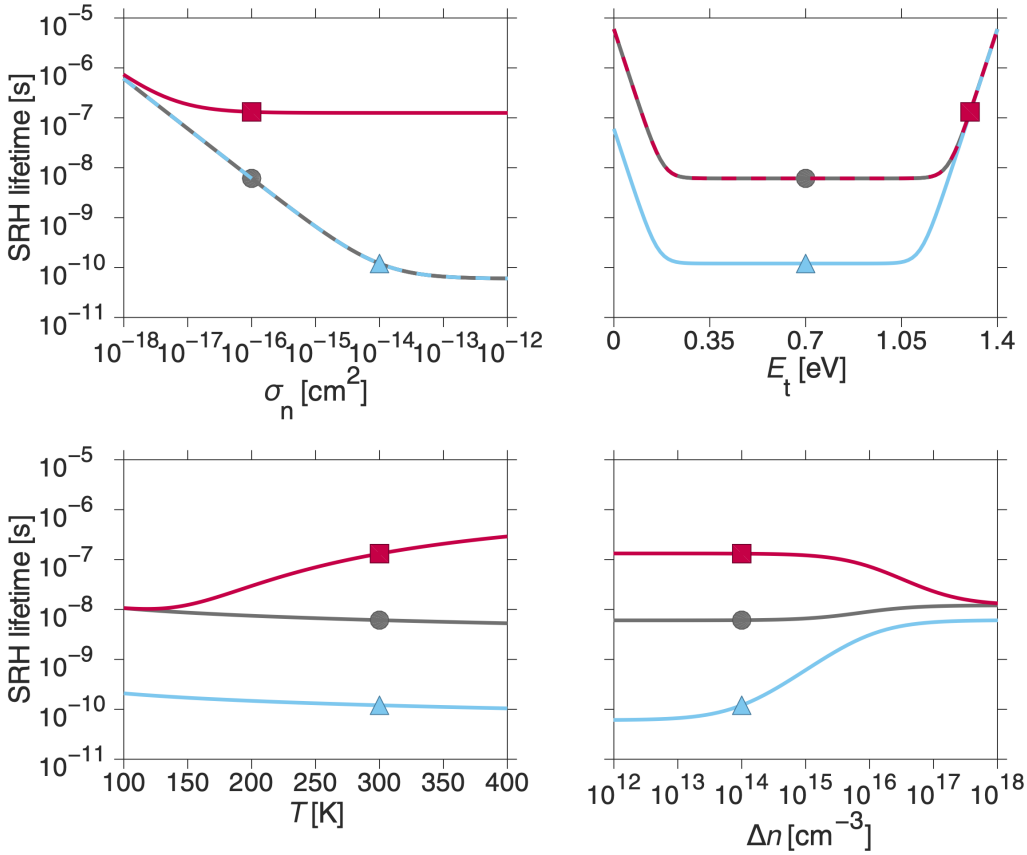

Figure S1: SRH lifetime sensitivity plots showing a baseline calculation (grey dot) along with variations in σ_n (blue) and E_t (red), also showing dependence on illumination (injection level Δn) and temperature.

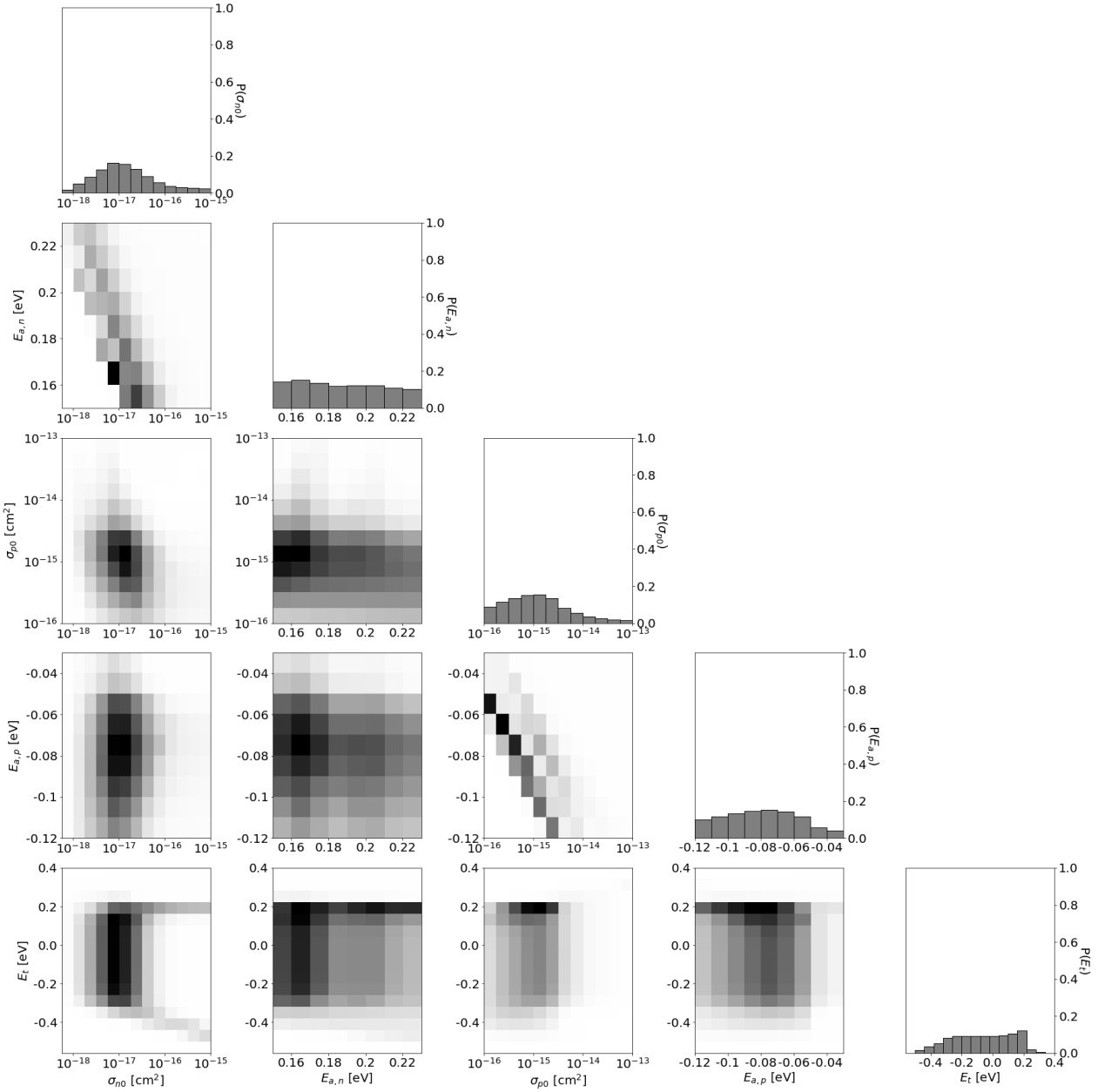

Figure S2: Full five-parameter probability distribution.

<table>
<tr><th>parameter name</th><th>value / setting</th><th>Ref.</th><th>notes</th></tr>
<tr><td>Device Area</td><td>3.55 cm^2</td><td>measured 4.00 cm^2; Ref. 1</td><td>adjusted downward from 4.00 cm^2 due to boundary effects (i.e., 1-Sun J_{SC} of real cell does not match QE-calculated J_{SC}). Partially because aperture is used during measurement.)</td></tr>
<tr><td>Surface texture</td><td>No surface texturing</td><td></td><td></td></tr>
<tr><td>Surface charge</td><td>No surface charge</td><td>2</td><td>Ref. 2 lists no surface charge for the conventional cell. A rear surface charge of 10^{10} cm^{-2} didn't seem to matter much, either. Also see PC1Dmod 6-2 manual, p. 13.</td></tr>
<tr><td>Reflectance: Front External</td><td>Coated; broadband reflectance = 0.69%; inner layer (thickness, index) = (76 nm, 1.98)</td><td>1</td><td>Used high end of thickness, 73±3 nm, to better fit reflectance data measured experimentally</td></tr>
<tr><td>Reflectance: Rear External</td><td>Fixed (0%)</td><td></td><td></td></tr>
<tr><td>Reflectance: Internal Reflectance</td><td>Front surface: specular, 30% (first bounce and subsequent bounces); Rear surface: specular, 95% (first bounce and subsequent bounces);</td><td></td><td>Adjusted to fit experimentally measured reflectance</td></tr>
<tr><td>Contact definition</td><td><table><tr><th></th><th>internal series resistance</th><th>distance from surface</th></tr><tr><td>emitter</td><td>$10^{-8}\Omega$</td><td>0 μm</td></tr><tr><td>base</td><td>0.18 Ω</td><td>400 μm</td></tr></table></td><td>base and emitter thickness: Ref. 1</td><td></td></tr>
<tr><td>Internal shunt element 1</td><td>conductor, 5.83×10^{-4}, anode/cathode/ideality = 400/0/1</td><td></td><td>Fitted to experimental J–V data</td></tr>
<tr><td>Global band structure</td><td>electron affinity: 4.05 eV</td><td></td><td>Other parameters defined by configuration file.</td></tr>
</table>

Table S1: PC1D **device** parameters for simulating *JVTi* data.

parameter name	**value / setting**	**Ref.**	**notes**
Thickness	400 μm	1	
Dielectric constant	11.7		
Optical properties: Refractive index–External	data file	3	
Optical properties: Intrinsic absorption – External absorption coeff.	data file	3	
Optical properties: Free-carrier absorption	Enabled; $\alpha = 2.85 \times 10^{-26} n\lambda^{2.6} + 1.64 \times 10^{-25} p\lambda^{2.4}$	4	
Background doping	p-type; 4.979×10^{15} cm^{-3}; resistivity = 2.85 Ω-cm	1	
First front diffusion	Enabled, n-type; calculated from Erfc, sheet resistance = 27.01, junction depth = 1.3 μm (peak doping / depth factor / and peak position = 1.062e20, 0.4516, 0)		Calculated in-program. Iterated the sheet resistance and depth factor to match the experimental QE.
Second front diffusion	No second front diffusion		
First/second rear diffusion	No rear diffusion		
Bulk recombination	fitting parameter		
Front surface	1×10^7 cm/s, $E_t = E_i$	suggested from Ref. 2	
Rear surface	1×10^7 cm/s, $E_t = E_i$	suggested from Ref. 2	

Table S2: PC1D **material** parameters for simulating *JVTi* data.

parameter name	**value / setting**	**notes**
Excitation mode	Transient, number of time steps = 100; time step size = 1 s; time step at t=0 = 1e-09	
Temperature	*input parameter*	
Base circuit	Source: 0 Ω-cm^2 resistance; sweep from −0.5 to +1.0 V	zero resistance necessary for voltage to sweep full range (vs. some subset)
Collector circuit	all parameters set to zero	
Primary illumination – intensity	Enable; Front; level is input parameter; AM1.5G spectrum	
Secondary illumination	disabled	

Table S3: PC1D **excitation** parameters for simulating *JVTi* data.

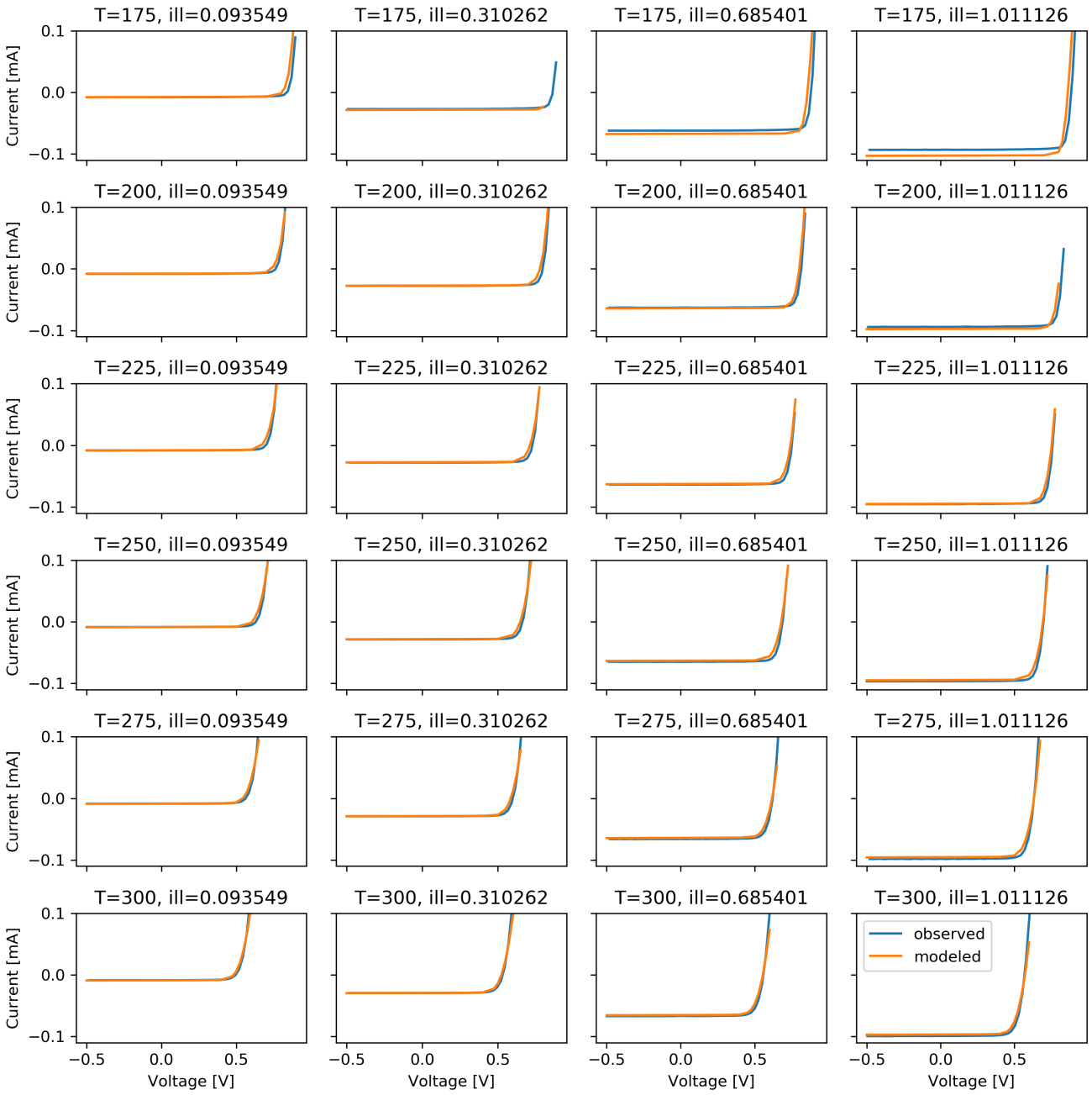

Figure S3: Comparison between modeled and simulated (for highest-probability set of Arrhenius parameters) at every experimental condition (illumination levels in Suns, temperatures in K). Lack of high-voltage data for some conditions was due to numerical convergence errors.

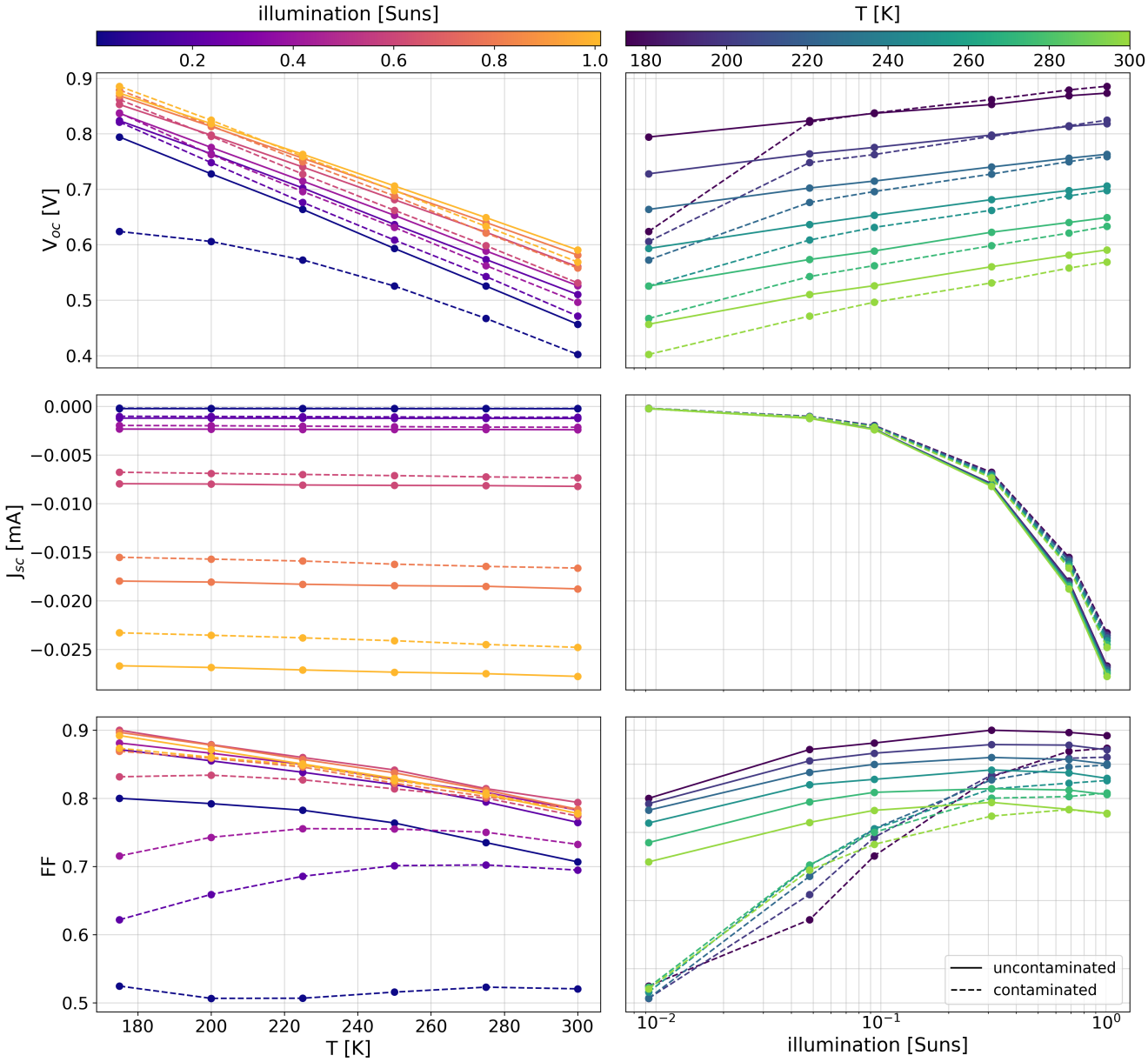

Figure S4: Open-circuit voltage (V_{oc}), short-circuit current (J_{sc}), and fill factor (FF) for contaminated (dotted line) and uncontaminated (solid line) samples plotted against temperature and illumination intensity, with values of other experimental condition in each case indicated by the colorbars.

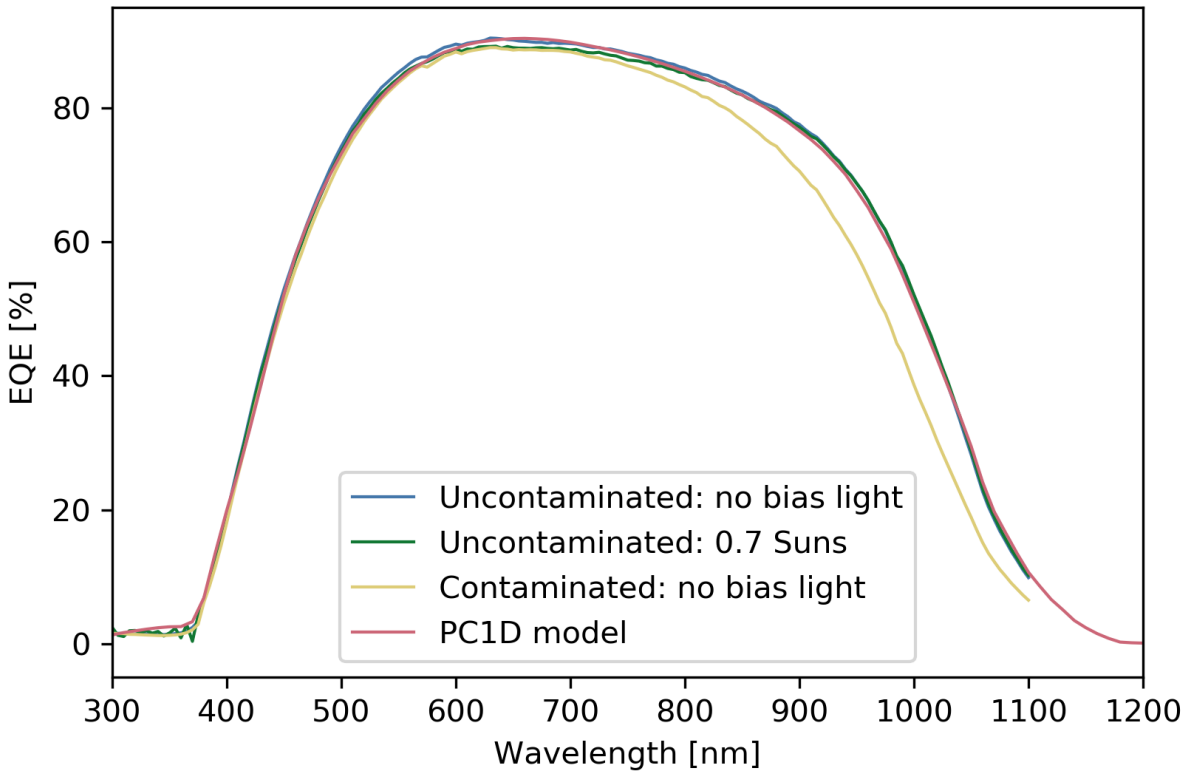

Figure S5: External quantum efficiency data with and without bias light for the uncontaminated sample, without bias light for contaminated sample, and PC1D model output for unbiased QE with parameters calibrated on uncontaminated sample.

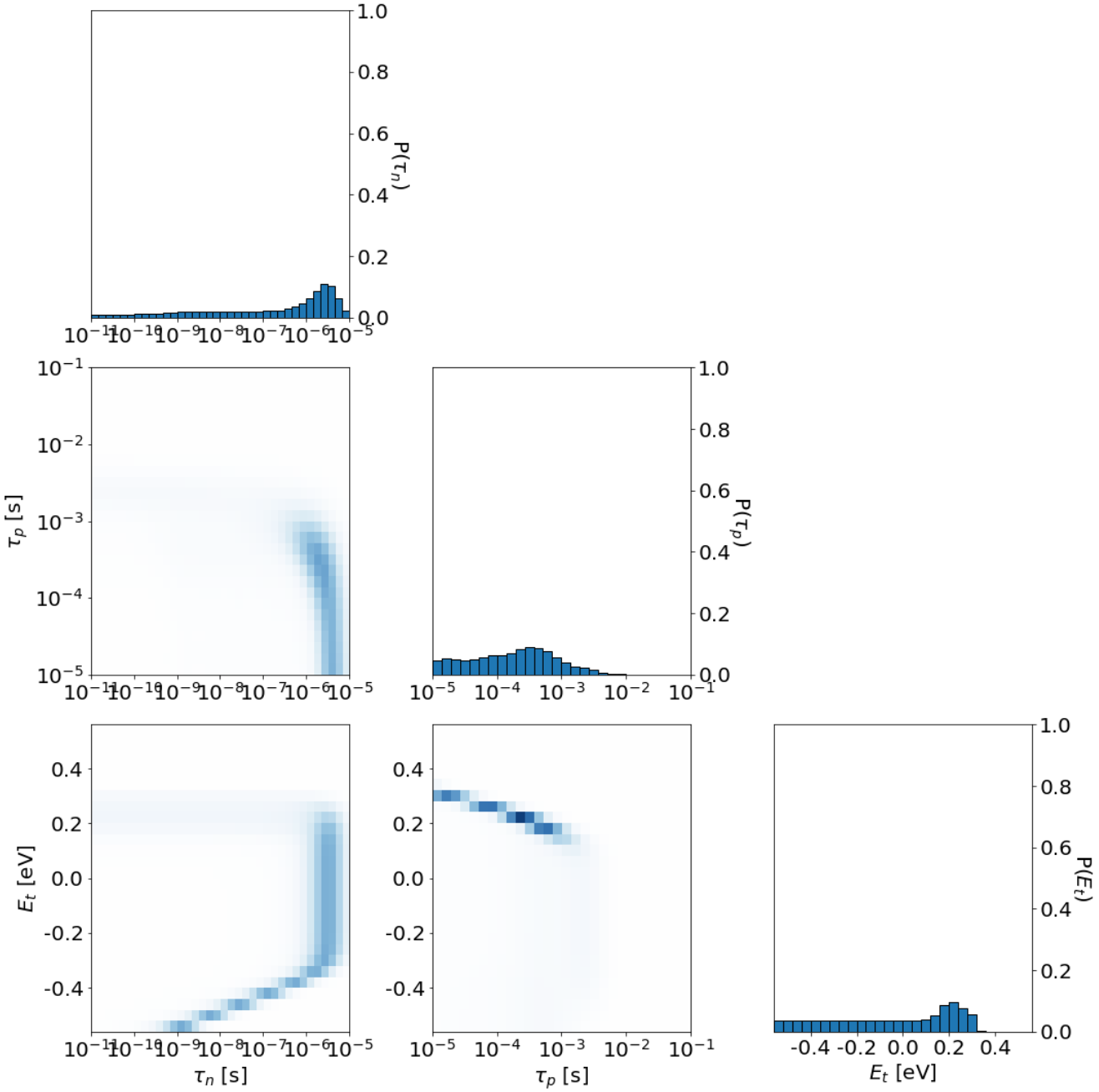

Figure S6: Results for the three-parameter fit at 300K using data only at 1 Sun light intensity.

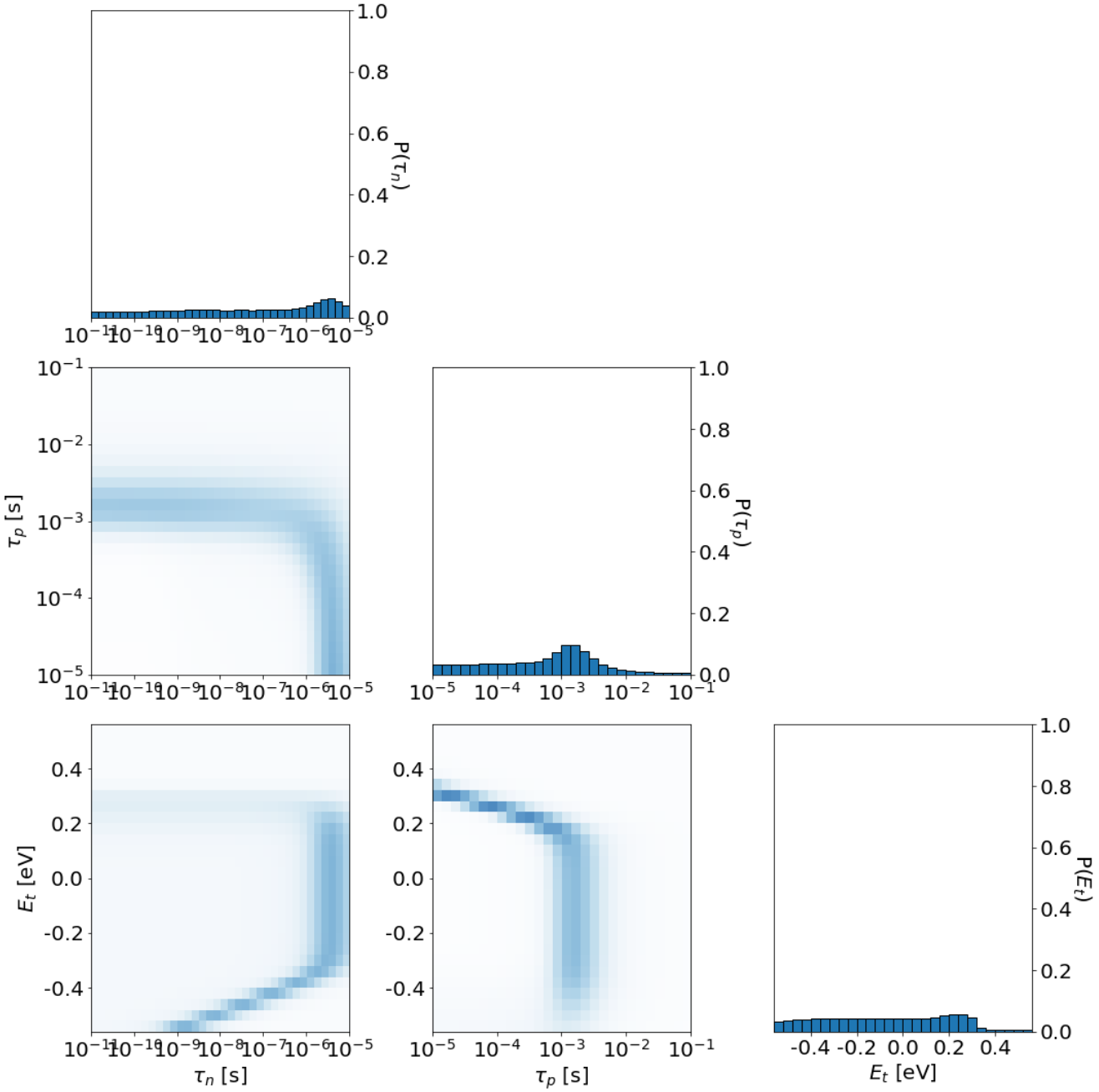

Figure S7: Results for the three-parameter fit at 300K using data only at V_{oc} for each JV curve.

References

[1] V. Vähänissi, A. Haarahiltunen, H. Talvitie, M. Yli-koski, and H. Savin, "Impact of phosphorus gettering parameters and initial iron level on silicon solar cell properties," *Progress in Photovoltaics: Reseach and Applications*, pp. 1127–1135, 2013.

[2] A. Fell, K. R. McIntosh, P. P. Altermatt, G. J. M. Janssen, R. Stangl, A. Ho-Baillie, H. Steinkemper, J. Greulich, M. Müller, B. Min, K. C. Fong, M. Hermle, I. G. Romijn, and M. D. Abbott, "Input parameters for the simulation of silicon solar cells in 2014," *IEEE Journal of Photovoltaics*, vol. 5, no. 4, pp. 1250–1263, July 2015.

[3] M. A. Green, "Self-consistent optical parameters of intrinsic silicon at 300k including temperature coefficients," *Solar Energy Materials and Solar Cells*, vol. 92, no. 11, pp. 1305 – 1310, 2008. [Online]. Available: http://www.sciencedirect.com/science/article/pii/S0927024808002158

[4] M. Rüdiger, J. Greulich, A. Richter, and M. Hermle, "Parameterization of free carrier absorption in highly doped silicon for solar cells," *IEEE Transactions on Electron Devices*, vol. 60, no. 7, pp. 2156–2163, July 2013.